A Study of Properties of the Ca^{2+}-Dependent Delayed Afterdepolarizations in a Mathematical Model for Human Ventricular Myocytes

Navneet Roshan[1] and Rahul Pandit[1]
[1] Centre for Condensed Matter Theory, Department of Physics, Indian Institute of Science, Bangalore, India

Abstract

Delayed afterdepolarizations (DADs), observed in cardiac myocytes can be arrhythmogenic. These DADs may arise in diseased conditions or mutations that induce numerous changes in the expression levels of exchangers, ion channels, or ionic pumps. It is difficult to reproduce these changes in experiments; therefore, we carry out a detailed in silico study of these modifications in the human ventricular myocyte model due to ten Tusscher and Panfilov (TP06). We find three types of DADs. Furthermore, by using parameter-sensitivity analysis, we show that the Na^+-Ca^{2+} exchanger and the SERCA pump uptake rate are the critical parameters for triggering DADs. We also show that the Na^+-Ca^{2+} conductance increases the DAD amplitude, whereas the SERCA uptake rate increases the frequency of the DADs. We obtain a phase diagram for the TP06 model and present regions of parameter space which show various types of DADs.

1. Introduction

Arrhythmogenic afterdepolarizations occur in the late phases of the cardiac action potential (AP). These afterdepolarizations are categorized into two types, depending upon the phase of the AP. The afterdepolarizations that occur during the plateau phase of the AP are called early afterdepolarizations (EADs); the ones that occur during the diastolic interval (DI) are called delayed afterdepolarizations (DADs). Experiments on mammalian hearts [1], such as *in vitro* studies in ferret [2] and cat [3] myocytes, suggest that DADs are triggered by Ca^{2+}-induced-Ca^{2+}-release (CICR), i.e., the release of Ca^{2+}-ions from ryanodine receptors (RyR) by the action of Ca^{2+} alone. During the diastolic interval, when L-type Ca^{2+} channels are closed, these CICR events lead to DAD, which are observed during the following heart conditions: a hypertrophied failing heart [4], the post-acidotic incidence of cardiac arrhythmias [5], and exercise-induced catecholaminergic polymorphic ventricular tachycardia(CPVT)[6]. These conditions are associated primarily with Ca^{2+}-overload and RyR mutations. One well-known mechanism for DADs is the leak of Ca^{2+} from these mutated RyRs. The Ca^{2+} leak from RyRs triggers other RyRs to open and generate spontaneous Ca^{2+} release, which is known as a Ca^{2+}-spark. Once a Ca^{2+}-spark occurs, the Ca^{2+}-concentration rises in the intracellular spaces. The Na^+-Ca^{2+} exchanger (NCX) senses the increased Ca^{2+} in the intracellular space and acts to evacuate the excess Ca^{2+}. The Electrogenic nature of the NCX (exchanges 1 Ca^{2+} ion for 3 Na^+ ions), depolarises the myocyte membrane. Given the strength of the Ca^{2+}-spark, the amplitude of the resultant DAD may depend on multiple parameters. DADs are conventionally divided into two types: a suprathreshold DAD, if it reaches the AP-excitation threshold, and subthreshold DADs, which do not reach the AP-excitation threshold. DADs are one of the known precursors of cardiac disturbances at the whole heart level, so it is vital to understand these DADs in cardiac-myocyte parameter space. We carry out such a study by using the TP06 model for human ventricular myocytes. Among the available models in the literature, only a few mathematical models can yield DADs as discussed in Ref. [7], which has classified the models capable of inducing DADs and methods to identify them. We organize our study as follows: Section 2 describes out Model and Methods. In Section 3 we give Results and Conclusions.

2. Model and Methods

2.1. Model description

We use the TP06 human ventricular myocyte model, for which we show the Ca^{2+}-subsystem via a schematic diagram in Fig. 1. The myocyte volume is divided into three compartments: SR is the sarcoplasmic reticulum volume, SS is the subspace volume, and CYTO is the cytoplasmic volume of the myocyte. The ordinary differential equation (ODE) for the membrane potential is

$$\frac{dV}{dt} = -\frac{I_{stim} + I_{ion}}{C_m}, \tag{1}$$

where V is the potential difference across the myocyte membrane, t is the time and C_m is the membrane capaci-

 ISSN: 2325-887X DOI: 10.22489/CinC.2021.205

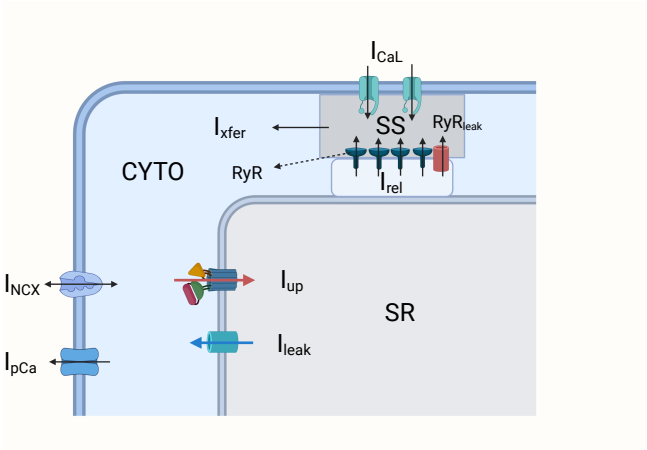

Figure 1. Schematic diagram of the TP06 model's Ca^{2+} subsystem. Here the myocyte volume is divided into three compartments: the sarcoplasmic reticulum (SR), the subspace (SS), and the cytoplasm (CYTO). RyRs are the ryanodine receptors, I_{rel} is the RyRs Ca^{2+}-release rate. SS is the volume where Ca^{2+}-induced-Ca^{2+}-release occurs. I_{up} is the SERCA pump uptake from the CYTO to the SR. I_{leak} is Ca^{2+}-leak from the SR to the CYTO, RyR_{leak} is Ca^{2+}-leak from the SR volume to the SS volume and I_{xfer} is diffusion flux of Ca^{2+}-ions from the SS to the CYTO. I_{pCa}, I_{NCX} and I_{CaL} are transmembrane currents. Figure created with BioRender.com.

tance. The TP06 model has 12 transmembrane ionic currents, and I_{ion} is the sum of all these currents:

$$I_{ion} = I_{Na} + I_{CaL} + I_{K1} + I_{Kr} + I_{Ks} + I_{to} + I_{pK} + I_{bCa} + I_{NaCa} + I_{NaK} + I_{bNa} + I_{pCa}. \quad (2)$$

These currents are as follows: the fast Na^+ current (I_{Na}); L-type Ca^{+2} (I_{CaL}); inward rectifier (I_{K1}); rapid-delayed rectifier (I_{Kr}); slow-delayed rectifier (I_{Ks}); transient-outward (I_{to}); plateau K^+ (I_{pK}); background Ca^{2+} (I_{bCa}); Na^+-Ca^{2+} exchanger (I_{NaCa}); Na^+-K^+ ATPase exchanger (I_{NaK}); Na^+ background (I_{bNa}); plateau Ca^{2+} current (I_{pCa}). The conductances for these currrents are G_{Na}, $G_{CaL}, G_{to}, G_{pK}, G_{bCa}, K_{NaCa}, P_{NaK}, G_{bNa}$ and G_{pCa}, respectively.

The detailed ODEs for the currents and Ca^{2+}-concentrations of the model are given in the Ref.[8]. In the equations for Ca^{2+} concentrations, there are equations for I_{rel} and I_{up}, which are the molar flow rates of Ca^{2+}-ions from the SR volume to the SS volume and CYTO to SR, respectively. We have modified the I_{rel} in this model by adding a small leak rate $0.00018 ms^{-1}$ as follows:

$$\begin{aligned} I_{rel} &= (V_{rel}.O + 0.00018)([Ca^{2+}]_{SR} - [Ca^{2+}]_{SS}) \\ I_{up} &= \frac{V_{maxup}}{1 + \frac{{K_{up}}^2}{{Ca_i}^2}}, \end{aligned} \quad (3)$$

where the control value of $V_{rel} = 0.102\ ms^{-1}$ and O is the probability of the RyR being open, $[Ca^{2+}]_{SR}$ and $[Ca^{2+}]_{SS}$ are molar concentrations in spaces SR and SS respectively. $V_{maxup} = 0.006375\ mM/ms$ is the control parameter for the SERCA uptake rate, $K_{up} = 0.00025\ mM$ and Ca_i is the Ca^{2+}-concentration in the CYTO. We use the numerical scheme from Ref. ([9]) to integrate Eq. (1) with the time step $\delta t = 0.02$ ms. In our simulations, the frequency of stimulation of I_{stim} is 1 Hz. All the results we show are recorded and analyzed after 500 APs.

2.2. Method for sensitivity analysis

We use sensitivity analysis to find out which parameters among all conductances or fluxes (e.g., G_{Na} and V_{maxup}) affect DADs the most. For calculating sensitivity values, we use the algorithm mentioned in Ref.[10]. We choose 500 randomly sampled scale factors for each one of these parameters; e.g., the scale factor for G_{Na} follows from $G_{Na} = S_{GNa} \times G_{NaC}$, where G_{NaC} is the control value for G_{Na} and S_{GNa} is the scale factor for G_{Na} [11]. We use similar notations for other conductances and fluxes. These scale factors are chosen from a log-normal distribution which we obtain from a Gaussian distribution with standard deviation $\sigma = 0.1$ and mean $\mu = 0$. For each set of parameters, we generate 500 APs, by stimulation, and record the last 10 APs. From the recorded APs we calculate the outputs and their Z-scores, i.e., $(x - \mu_x)/\sigma_x$. For every output x, μ_x is the mean and σ_x is the standard deviation; we consider two outputs, namely, the amplitude and frequency of the DADs (DAD_{amp} and DAD_{freq}). To observe DADs in our sensitivity simulations, we use $S_{GCaL} = 2$ and $S_{Vmaxup} = 3$.

3. Results and Conclusion

3.1. Role of leak current

In Fig. 2 we present two channel plots without and with RyR-leak modifications; Figs. 2(a) and 2(b) shows plots of the AP; Figs. 2(c) and 2(d) show plots for NCX (I_{NaCa}); Figs. 2(e) and 2(f) shows plots of I_{rel}. In Figures 2(c) and 2(d) elucidates the role of NCX(I_{NaCa}) in depolarising the membrane once Ca^{2+}-sparks occur. Sharp peaks of I_{rel} in Fig. 2(f) are Ca^{2+}-sparks; note that the Ca^{2+}-spark at about 600 ms is associated with a DAD in Fig. 2(b).

3.2. Sensitivity analysis

The three types of DADs we have studied are shown in Fig. 3: (a) subthreshold DADs [Fig. 3(d)]; (b) multi-blip DADs [Fig. 3(e)]; (c) suprathreshold DADs [Fig. 3(f)].

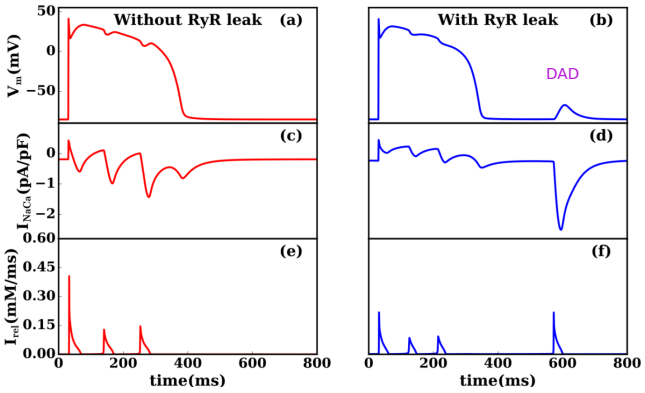

Figure 2. Two channel plots without and with RyR-leak modifications. We use scale factors ($S_{GCaL} = 2$,$S_{Vmaxup} = 3$) for both the channels. (a)-(b): Show plots of membrane potential. (c)-(d): Show plots for NCX (I_{NaCa}) role in depolarising membrane when Ca^{2+}-sparks occurred. (e)-(f): Show Ca^{2+} release I_{rel} from RyR.

To determine in which parameter ranges these DADs occur, we have carried out a sensitivity analysis (Sec. 2.2) to determine the parameters that affect the frequency and amplitude of these DADs crucially.

Results from our sensitivity analysis indicate that K_{NaCa}, G_{K1}, V_{maxup} affect the amplitude of DADs sensitivily. For the DAD frequency V_{maxup} and K_{NaCa} are the most sensitive parameters as we show Table[1]. Even though in the TP06 model V_{rel} determines the amplitude of the RyR release I_{rel}, our sensitivity results show that V_{rel} has a negligible effect on DAD_{amp} and DAD_{freq}.

DAD_{amp}		DAD_{freq}	
Rel. sens.	Biomarkers	Rel. sens.	Biomarkers
0.6508	K_{NaCa}	0.7497	V_{maxup}
0.1865	G_{CaL}	0.2342	G_{bCa}
-0.4713	V_{maxup}	-0.2302	G_{Kr}
-0.6697	G_{K1}	-0.3848	K_{NaCa}

Table 1. Relative sensitivities (Rel. sens.) of the most sensitive biomarkers for the amplitude and frequency of DADs, i.e., DAD_{amp} and DAD_{freq} respectively. Positive Rel. sens. indicate that increase in biomarkers increases the corresponding observables (DAD_{amp} and DAD_{freq}), whereas negative rel. sens. Indicates an increase in biomarkers will decrease the observable value.

3.3. Phase diagrams

In Fig. 3(a), we show how we can increase G_{CaL} and G_{Kr} to obtain Ca^{2+}-overload without changing the AP duration. This Ca^{2+}-overload is required for triggering DADs in the TP06 model. By enhancing Ca^{2+}-overload we observe three types of DADs in the TP06 model [see Figs. 3(d)-(f)]. In our future detailed study we will show various other phase diagrams.

In Fig. 3(b) we show an illustrative phase diagram in the S_{KNaCa}, S_{Vmaxup} parameter space, where cyan, blue, magenta and red regions yield the APs shown in Figs. 3(c), 3(d), 3(e) and 3(f), respectively.

We will present other phase diagram in our future detailed study.

3.4. Conclusions

It is important to understand the parameter-dependence of DADs, as they are known to be arrhythmogenic. We have carried out such a study for the TP06 mathematical model for human ventricular myocytes. Our study re-emphasizes the role of the RyR-leak in forming such DADs. Our sensitivity analysis in Table[1] helps us to identify the principal parameters that affect DAD_{amp} and DAD_{freq} in the TP06 model (Table [1]). Phase diagrams, such as the one we give in Fig. 3(b), help us to identify the parameter regions in which we obtain three types of DADs.

3.5. Limitations of our study

In the model we have studied, the distribution of the Na^{+}-Ca^{2+} exchanger is limited only to the cytoplasm; however, in more realistic models, e.g., in Ref.[12], the Na^{+}-Ca^{2+} exchanger is distributed in other compartments also. We will report our results in detailed studies. The model We have studied is a common-pool model which lacks the description of spatial details inside myocyte.

Acknowledgements

We thank the Department of Science and Technology (DST), India, and the Council for Scientific and Industrial Research (CSIR), India, for financial support, and the Supercomputer Education and Research Centre (SERC, IISc) for computational resources. We thank Mahesh K. Mulimani and Soling Zimik for valuable discussions.

References

[1] Kass RS, Tsien RW. Fluctuations in membrane current driven by intracellular calcium in cardiac purkinje fibers. Biophysical journal 1982;38(3):259–269.

[2] Marban E, Robinson SW, Wier WG, et al. Mechanisms of arrhythmogenic delayed and early afterdepolarizations in ferret ventricular muscle. The Journal of clinical investigation 1986;78(5):1185–1192.

[3] Kimura S, Cameron J, Kozlovskis P, Bassett A, Myerburg R. Delayed afterdepolarizations and triggered activity induced in feline purkinje fibers by alpha-adrenergic stimula-

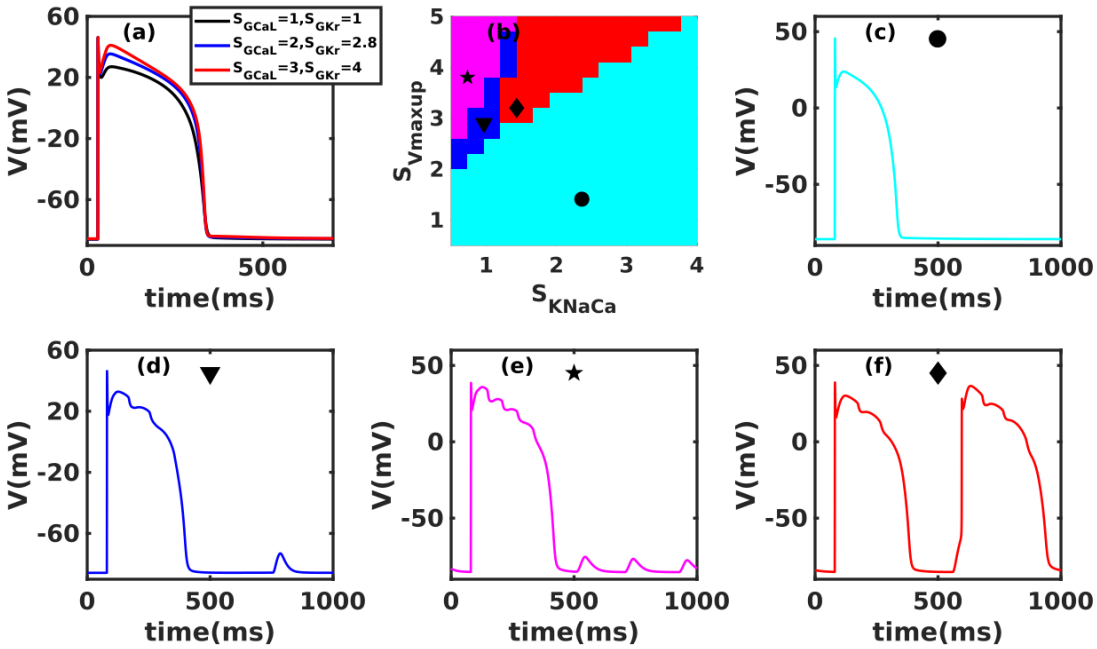

Figure 3. (a): AP plots for different values of S_{GCaL} and S_{GKr} (b): Phase diagram in the : S_{KNaCa} and S_{Vmaxup} parameter space for various types of DADs at $S_{GCaL} = 2$. Where cyan, blue, magenta and red regions yield the APs shown in (c): Normal action potential. (d): Subthreshold DAD. (e): Multi-blip DAD. (f): Suprathreshold DAD.

tion in the presence of elevated calcium levels. Circulation 1984;70(6):1074–1082.

[4] de Groot SM, Schoenmakers M, Molenschot MM, Leunissen JD, Wellens HJ, Vos MA. Contractile adaptations preserving cardiac output predispose the hypertrophied canine heart to delayed afterdepolarization–dependent ventricular arrhythmias. Circulation 2000;102(17):2145–2151.

[5] Pogwizd SM, Onufer JR, Kramer JB, Sobel BE, Corr PB. Induction of delayed afterdepolarizations and triggered activity in canine purkinje fibers by lysophosphoglycerides. Circulation research 1986;59(4):416–426.

[6] Leenhardt A, Lucet V, Denjoy I, Grau F, Ngoc DD, Coumel P. Catecholaminergic polymorphic ventricular tachycardia in children: a 7-year follow-up of 21 patients. Circulation 1995;91(5):1512–1519.

[7] Fink M, Noble PJ, Noble D. Ca2+-induced delayed afterdepolarizations are triggered by dyadic subspace ca2+ affirming that increasing serca reduces aftercontractions. American Journal of Physiology Heart and Circulatory Physiology 2011;301(3):H921–H935.

[8] Ten Tusscher KH, Panfilov AV. Alternans and spiral breakup in a human ventricular tissue model. American Journal of Physiology Heart and Circulatory Physiology 2006;291(3):H1088–H1100.

[9] Mulimani MK, Nayak AR, Pandit R. Comparisons of wave dynamics in hodgkin-huxley and markov-state formalisms for the sodium (na) channel in some mathematical models for human cardiac tissue. Physical Review Research 2020; 2(3):033443.

[10] Sobie EA. Parameter sensitivity analysis in electrophysiological models using multivariable regression. Biophysical journal 2009;96(4):1264–1274.

[11] Mulimani MK, Zimik S, Pandit R. An in silico study of electrophysiological parameters that affect the spiral-wave frequency in mathematical models for cardiac tissue. arXiv preprint arXiv210806531 2021;.

[12] Himeno Y, Asakura K, Cha CY, Memida H, Powell T, Amano A, Noma A. A human ventricular myocyte model with a refined representation of excitation-contraction coupling. Biophysical journal 2015;109(2):415–427.

Address for correspondence:

Navneet Roshan, navneetroshanp@gmail.com, navneet@iisc.ac.in; Department of Physics, IISc, Bangalore, India

Rahul Pandit, rahul@iisc.ac.in; also at Jawaharlal Nehru Centre For Advanced Scientific Research, Jakkur, Bangalore, India